Dark state polarizing a nuclear spin in the vicinity of a nitrogen-vacancy center

Yang-Yang Wang (王洋洋),[1] Jing Qiu (邱静),[1] Ying-Qi Chu (褚莹琦),[1] Mei Zhang (章梅),[1] Jianming Cai (蔡建明),[2,3] Qing Ai (艾清),[1,*] and Fu-Guo Deng (邓富国)[1]

[1]*Department of Physics, Applied Optics Beijing Area Major Laboratory, Beijing Normal University, Beijing 100875, China*
[2]*School of Physics and Center for Quantum Optical Science, Huazhong University of Science and Technology, Wuhan 430074, China*
[3]*International Joint Laboratory on Quantum Sensing and Quantum Metrology, Huazhong University of Science and Technology, Wuhan 430074, China*

(Received 20 August 2017; revised manuscript received 17 March 2018; published 10 April 2018)

The nuclear spin in the vicinity of a nitrogen-vacancy (NV) center possesses long coherence time and convenient manipulation assisted by the strong hyperfine interaction with the NV center. It is suggested for the subsequent quantum information storage and processing after appropriate initialization. However, current experimental schemes are either sensitive to the inclination and magnitude of the magnetic field or require thousands of repetitions to achieve successful realization. Here, we propose a method to polarize a ^{13}C nuclear spin in the vicinity of an NV center via a dark state. We demonstrate theoretically and numerically that it is robust to polarize various nuclear spins with different hyperfine couplings and noise strengths.

DOI: 10.1103/PhysRevA.97.042313

I. INTRODUCTION

Benefiting from quantum entanglement [1,2], quantum information processing can effectively speed up computation and ensure security of information [3]. As the basic element, the quantum bit (qubit) lies at the heart of quantum information processing [3,4]. Solid-state qubits are a promising candidate because they might well explore the well-developed technology of the semiconductor industry [5,6]. Remarkably, the nitrogen-vacancy (NV) center in diamond has been recognized as an intriguing choice since it is of easy accessibility and long coherence time at room temperature [7–11]. To date, various applications including quantum information processing and quantum metrology have been successfully realized in the NV centers [12–14]. For example, different versions of transitionless driving algorithms have been fully utilized to accelerate quantum control in the NV centers [15–18]. Besides, the NV centers have been explored to probe the internal dynamics of clusters of nuclear spins by dynamical decoupling [19,20]. The NV center has also been proposed to detect the radical-pair chemical reaction in biology [21] and weak magnetic fields [22]. Due to the quantum nature of the surrounding nuclear-spin bath, the anomalous decoherence effect of the NV center has been theoretically predicted [23] and experimentally verified [24].

Apart from the electron spin of the NV center, the nuclear spins in the vicinity of an NV center is of broad interest to the community. Due to much longer coherence time, nuclear spins are more frequently used in quantum information storage and processing [25–33]. However, it is difficult to initialize and control the nuclear spins because of their small magnetic moments. Utilizing an ancillary electronic spin to couple with the nuclear spin by the hyperfine interaction may effectively overcome this limitation.

To our best knowledge, there are three kinds of experimental schemes which have been successfully demonstrated to initialize the nuclear spins around NV centers. A straightforward approach is to repeatedly perform projective measurements until the desired state is observed [28,29]. An alternative is to bring the excited (ground) state close to the level-anticrossing point by applying a specific static magnetic field [27,34]. In the last but widely used approach [25,26,31,35,36], the electron spin is first initialized, and then its polarization is coherently swapped to the nuclear spin. After tens of repetitions of the above process, nearly complete polarizations of both electronic and nuclear spins are achieved. Here, we remark that in each repetition the swapping of polarization between the electron and nuclear spins is essentially a quantum-state transfer process.

For any state transfer process, the fidelity is inevitably influenced by the noise due to coupling to the bath. On the other hand, we notice that the dark state has been extensively applied to coherently transfer energy in photosynthetic light harvesting [37] and to perfectly transfer state in optomechanical systems [38,39]. The coherent coupling between a surface acoustic wave and an NV center was experimentally realized via the dark state recently [40]. Inspired by these discoveries, we theoretically propose a method to polarize a ^{13}C nuclear spin in the vicinity of an NV center by the dark state. To create the dark state for the state transfer, two-photon resonance is required, i.e., $\Delta = 0$. The transfer fidelity is further optimized by one-photon resonance, i.e., $\delta = 0$. In order to provide an effective guidance for the experimental realization, we perform an analytical analysis on the probability of the nuclear-spin-polarized state by the Schrödinger equation with a non-Hermitian Hamiltonian. It is shown that when the Rabi frequencies of the two pulses are equal, the polarization is predicted to reach the maximum at

*aiqing@bnu.edu.cn

the given time. Further numerical simulation demonstrates an anomalous effect whereby the polarization of a nuclear spin with a smaller hyperfine interaction can be even higher than a nuclear spin at the nearest-neighbor site due to the transverse hyperfine interaction. Compared with the above methods, our scheme works effectively over a broad range of magnetic field and only a few repetitions are required.

II. SYSTEM MODEL

As shown in Fig. 1(a), the NV center in diamond with a C_{3v} symmetry consists of a nitrogen atom associated with a vacancy in an adjacent lattice site. For the negatively charged NV center with electron spin $S = 1$, the ground state is a spin-triplet state ^{3}A, with a zero-field splitting $D = 2.87$ GHz [1] between spin sublevels $m_s = 0$ and $m_s = \pm 1$ due to the electronic spin-spin interaction. In this article, we consider a first-shell ^{13}C nuclear spin coupled with the electronic spin of an NV center. As a result, there is a strong hyperfine coupling $A_\parallel = 130$ MHz [41] between the nuclear and electronic spins. Figure 1(b) shows the energy-level diagram of the ground-state hyperfine structure associated with a nearby ^{13}C nuclear spin. We label the states of this bipartite system as $|m_s,\uparrow\rangle$ and $|m_s,\downarrow\rangle$, where $|\uparrow\rangle$ and $|\downarrow\rangle$ are the nuclear-spin states.

We consider a weak static magnetic field $B_z < 673$ G along the NV principle axis by a permanent magnet. The total Hamiltonian of the electron-spin ground state and a nearby ^{13}C nuclear spin reads [31]

$$H_F = DS_z^2 + \gamma_e B_z S_z + \gamma_c B_z I_z + A_\parallel S_z I_z + A_\perp (S_x I_x + S_y I_y). \quad (1)$$

Here, S_α and I_α ($\alpha = x,y,z$) are respectively the electron- and nuclear-spin operators. The first term stands for the zero-field splitting of the electronic ground state. The following two terms, $\gamma_e B_z S_z$ and $\gamma_c B_z I_z$, are the electron- and nuclear-spin Zeeman energy splittings with the electronic gyromagnetic ratio $\gamma_e = -1.76\times10^{11}$ rad s^{-1} T^{-1} [42] and the nuclear gyromagnetic ratio $\gamma_c = 6.73\times10^{7}$ rad s^{-1} T^{-1} [23]. The last two terms describe the hyperfine interaction between the electron spin and the ^{13}C nuclear spin, where $A_\parallel$ and $A_\perp$ are the longitudinal and transverse hyperfine interactions, respectively.

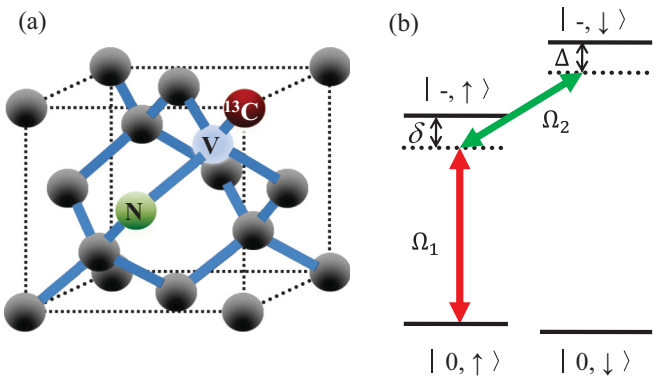

FIG. 1. Schematic of polarizing a ^{13}C nuclear spin in the vicinity of an NV center. (a) The structure of an NV center. (b) Energy levels of the electron and ^{13}C nuclear spins under the hyperfine interaction. Two pulses are simultaneously applied to induce the transitions of $|0,\uparrow\rangle \leftrightarrow |-,\uparrow\rangle$ and $|-,\uparrow\rangle \leftrightarrow |-,\downarrow\rangle$ with respectively Rabi frequencies Ω_1 and Ω_2, and one-photon detuning δ, and two-photon detuning Δ.

Due to the weak magnetic field strength, the relevant level spacings are much larger than the transverse hyperfine interaction, i.e., $|D - \gamma_e B_z + \gamma_c B_z - \frac{1}{2}A_\parallel| \gg A_\perp/\sqrt{2}$. Therefore, the $S_x I_x$ and $S_y I_y$ terms of the hyperfine interaction are totally negligible. In this case, the secular approximation is valid [25,35,43,44] and only the longitudinal hyperfine interaction is taken into account. In the absence of time-varying magnetic fields, the Hamiltonian can be approximated as

$$H_F^S \simeq DS_z^2 + \gamma_e B_z S_z + \gamma_c B_z I_z + A_\parallel S_z I_z. \quad (2)$$

III. POLARIZING BY DARK STATE

As shown in Fig. 1(b), the transition $|0,\uparrow\rangle \leftrightarrow |-,\uparrow\rangle$ is addressed via a microwave pulse with Rabi frequency Ω_1 and driving frequency $\omega_A = D - \gamma_e B_z - \delta - A_\parallel/2$, while the transition $|-,\uparrow\rangle \leftrightarrow |-,\downarrow\rangle$ is driven via a radio-frequency pulse with Rabi frequency Ω_2 and driving frequency $\omega_B = A_\parallel - \gamma_c B_z + \delta - \Delta$. Thus, in the presence of the two pulses the whole Hamiltonian of the system reads $H_M = H_F + H_I$, where the interaction Hamiltonian after a rotating-wave approximation that eliminates the fast-oscillating terms is

$$H_I = \Omega_1 e^{i\omega_A t}|0,\uparrow\rangle\langle -,\uparrow| + \Omega_2 e^{i\omega_B t}|-,\uparrow\rangle\langle -,\downarrow| + \text{H.c.} \quad (3)$$

Hereafter, we demonstrate polarizing the nuclear spin by the dark state. The nuclear and electronic spins are initially in a product state [26,29,31]. In each cycle there are two steps. First of all, the system evolves under the influence of the simultaneous microwave and radio-frequency pulses. In the second step, the electronic and nuclear spins are decoupled by a 532-nm optical pumping which reinitializes the electron spin in its ground state $|0\rangle$, while the state of the nuclear spin is unchanged, i.e., $\rho(t) \to \rho_e(0) \otimes \text{Tr}_e\rho(t)$ [26,29]. Then, the above cycle is repeated until a high polarization of the nuclear spin is reached.

The optical excitation with a 532-nm laser pulse leads to a strong spin polarization into the $|0\rangle$ sublevel of the ground state [1], which derives from spin-selective nonradiative intersystem crossing to a metastable state between the ground and excited triple states. In this sense, it is reasonable to choose the electronic initial state $\rho_e(0) = |0\rangle\langle 0|$. Due to the small nuclear Zeeman energy splitting with respect to the thermal energy, the nuclear spin is in the maximum mixed state $\rho_c(0) = (|\uparrow\rangle\langle\uparrow| + |\downarrow\rangle\langle\downarrow|)/2$. When the electronic spin is populated in $m_s = 0$, the longitudinal hyperfine interaction vanishes. Thus, the initial state of the total system is given by

$$\rho(0) = \rho_e(0) \otimes \rho_c(0). \quad (4)$$

Then, the microwave pulse and the radio-frequency pulse drive the transitions $|0,\uparrow\rangle \leftrightarrow |-,\uparrow\rangle$ and $|-,\uparrow\rangle \leftrightarrow |-,\downarrow\rangle$, respectively, with the different detunings δ and Δ. The total system evolves under the Hamiltonian $H_M = H_F + H_I$ for a time interval t. Since the total Hamiltonian H_M is time dependent, it is transformed to the rotating frame defined by $|\Psi(t)^R\rangle = U^\dagger(t)|\Psi(t)\rangle$ with $U(t) = \exp[-i(H_F^S - \delta|-,\uparrow\rangle\langle -,\uparrow| - \Delta|-,\downarrow\rangle\langle -,\downarrow|)t]$. Here, $|\Psi(t)^R\rangle$ satisfies the

Schrödinger equation in the rotating frame with the effective Hamiltonian

$$\begin{aligned} H_M^R &\equiv U^\dagger\big(H_F^S + H_I\big)U + iU^\dagger U \\ &= \delta|-,\uparrow\rangle\langle-,\uparrow| + \Delta|-,\downarrow\rangle\langle-,\downarrow| \\ &\quad + \Omega_1|0,\uparrow\rangle\langle-,\uparrow| + \Omega_2|-,\uparrow\rangle\langle-,\downarrow| + \text{H.c.} \end{aligned} \tag{5}$$

Generally speaking, the quantum dynamics of the electron and nuclear spins is subject to the noise, which can be described by the master equation

$$\partial_t\rho = -i[H_M,\rho] + \mathcal{L}\rho, \tag{6}$$

where $\mathcal{L}\rho = \kappa(|-\rangle\langle-|\rho|-\rangle\langle-| - \frac{1}{2}\{|-\rangle\langle-|,\rho\})$ describes the decoherence induced by the bath with κ being the decoherence rate, and $\{\cdot,\rho\}$ the anticommutator. Because in many cases T_1 is much longer than $T_2 = \kappa^{-1}$ [45–47], without loss of generality, we only take the pure-dephasing process into consideration in our simulation.

When the decoherence is sufficiently slow as compared to the coherent process described by H_M, the quantum jump term $|-\rangle\langle-|\rho|-\rangle\langle-|$ can be neglected. Thus, the total quantum dynamics including the decoherence can be simulated by the Schrödinger equation with a non-Hermitian Hamiltonian [37,48]

$$H = H_M^R - \frac{i}{2}\kappa|-\rangle\langle-|. \tag{7}$$

Because we apply two selective-resonance drivings to the NV center, the state $|0,\downarrow\rangle$ is sufficiently independent from the other three states. Therefore, hereafter we can separately consider the quantum dynamics of an initial state $|\psi(0)\rangle = |0,\uparrow\rangle$ driven by two driving pulses. As presented in the Appendix, at any time the state of the system reads

$$|\psi(t)\rangle = \sum_{j=1}^{3}\frac{N_j e^{-ix_j t}}{\prod_{k\neq j}(x_j - x_k)}|E_j\rangle, \tag{8}$$

where the three eigenstates of H are

$$\begin{aligned} |E_j\rangle = \frac{1}{N_j}\Big\{&\big[(x_j-\omega_1)(x_j-\omega_2) - \Omega_2^2\big]|0,\uparrow\rangle \\ &+ \Omega_1(x_j-\omega_2)|-,\uparrow\rangle + \Omega_1\Omega_2|-,\downarrow\rangle\Big\}, \end{aligned} \tag{9}$$

wherein N_j's are the normalization constants, x_j's are the eigenenergies, $\omega_1 = \delta - i\kappa/2$, and $\omega_2 = \Delta - i\kappa/2$. We employ two strong drivings to polarize the nuclear spin, i.e., $\omega_1,\omega_2 \ll \Omega_1,\Omega_2$. When the two-photon transition is resonant, i.e., $\Delta = 0$,

$$|E_1\rangle \simeq \frac{\Omega_2}{N_1}(-\Omega_2|0,\uparrow\rangle + \Omega_1|-,\downarrow\rangle) \tag{10}$$

is the dark state because it lacks the component of the lossy intermediate state $|-,\uparrow\rangle$, while

$$|E_2\rangle \simeq \frac{\Omega_1}{N_2}(\Omega_1|0,\uparrow\rangle + \Omega|-,\uparrow\rangle + \Omega_2|-,\downarrow\rangle), \tag{11}$$

$$|E_3\rangle \simeq \frac{\Omega_1}{N_3}(\Omega_1|0,\uparrow\rangle - \Omega|-,\uparrow\rangle + \Omega_2|-,\downarrow\rangle), \tag{12}$$

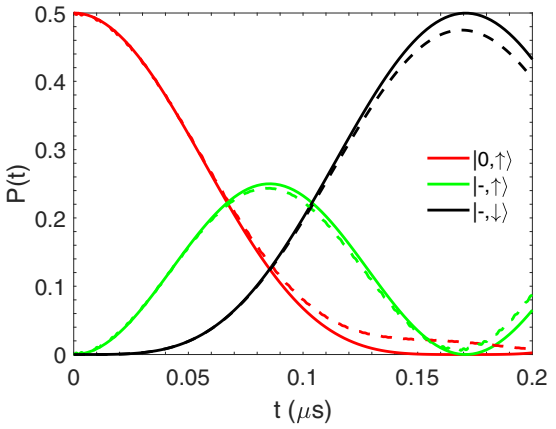

FIG. 2. The population dynamics of initial state $|0,\uparrow\rangle$ (red), intermediate state $|-,\uparrow\rangle$ (green), and target state $|-,\downarrow\rangle$ (black) by the Schrödinger equation (solid lines) with a non-Hermitian Hamiltonian expressed by Eq. (7) and the exact master equation with the exact Hamiltonian H_M (dashed lines). The population dynamics are drawn with $A_\parallel = 130$ MHz [49], $\delta = \Delta = 0$, $\Omega_1 = \Omega_2 = 13$ MHz, and $\kappa = 1/58$ MHz [50].

are the bright states suffering from relaxation. In this case, the state of the system is simplified as

$$\begin{aligned} |\psi(t)\rangle = &\frac{\Omega_1}{\sqrt{2}\Omega}e^{-i\frac{1}{2}(\omega_1+\frac{\Omega_2^2}{\Omega^2}\omega_2)t}(e^{-i\Omega t}|E_2\rangle + e^{i\Omega t}|E_3\rangle) \\ &-\frac{\Omega_2}{\Omega}e^{-i\frac{\Omega_1^2}{\Omega^2}\omega_2 t}|E_1\rangle \end{aligned} \tag{13}$$

with

$$\Omega = \sqrt{\Omega_1^2 + \Omega_2^2}. \tag{14}$$

By solving the Schrödinger equation with a non-Hermitian Hamiltonian expressed by Eq. (7), we numerically simulate the population dynamics of all three states for the resonance case, i.e., $\delta = \Delta = 0$, as shown by the solid lines in Fig. 2. In one cycle, almost 100% population in $|0,\uparrow\rangle$ can be coherently transferred to $|-,\downarrow\rangle$ even in the presence of noise. In order to derive the non-Hermitian Hamiltonian, several approximations have been utilized, i.e., dropping the quantum jump terms in the master equation, ignoring the transverse hyperfine interactions, and disregarding transitions due to the large-detuning condition. In order to validate these approximations, we also present the numerical simulation with the dashed lines in Fig. 2 by the exact master equation without the above approximations. Obviously, the differences between the two approaches are relatively small. Thus, it is valid to describe theoretically the quantum dynamics of the nuclear-spin polarization in the presence of noise via solving the Schrödinger equation with a non-Hermitian Hamiltonian.

By means of the Schrödinger equation with a non-Hermitian Hamiltonian, we can effectively analyze the effects of parameters on the nuclear-spin polarization and obtain a set of optimal parameters to guide the experiment for different conditions of nuclear spins. In the previous experimental realizations (cf. Refs. [25,26,31,35,36]), two π pulses are sequentially applied to swap the electron-spin polarization into the nuclear-spin polarization. Compared to this separate-pulse method [31],

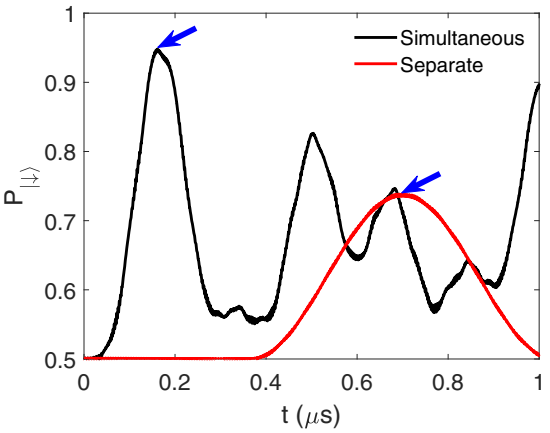

FIG. 3. Comparison between the probabilities of the nuclear spin in the $|\downarrow\rangle$ vs time by applying two simultaneous pulses (black line) and two separate pulses (red line). In the simultaneous case, $\Omega_1 = \Omega_2 = 13$ MHz, while $\Omega_1 = \Omega_2 = 4.3$ MHz [31] in the separate case. Other parameters are the same in both cases, i.e., $A_\parallel = 130$ MHz [49], $\delta = \Delta = 0$, and $\kappa = 1/58$ MHz [50]. The optimal operation times are labeled by the blue arrows.

the biggest difference is that we simultaneously apply two balanced pulses, and the strengths of pulses in our approach have an upper limit which is determined by the selective-excitation condition (see Sec. IV). Meanwhile, it implies that the operation time to polarize the nuclear spin is smaller than theirs, as presented in Fig. 3, i.e., 0.16 μs vs 0.7 μs. Second, our proposal makes full use of the dark state to avoid the noise suffered by the intermediate state; thus, the nuclear-spin polarization in our proposal is much higher than theirs as shown in Fig. 3 with the first peaks (i.e., 0.94 vs 0.7) indicated by the blue arrows via the different pulse ways. Therefore, the polarization for our proposal can achieve an optimal level by choosing optimal parameters to increase the polarization and reduce the swapping time.

The swapping of electron-spin polarization into nuclear-spin polarization is intrinsically a quantum-state transfer process from $|0,\uparrow\rangle$ to $|-,\downarrow\rangle$ via a lossy state $|-,\uparrow\rangle$. Intuitively, the fidelity of state transfer is subject to the noise strength. In Fig. 4(a), we explore the noise's effect on the fidelity of nuclear spin in the state $|\downarrow\rangle$ with $\kappa = 1$ MHz for different nuclear spins, i.e., different hyperfine interactions. For a nuclear spin in the first shell, the probability in $|\downarrow\rangle$ vs time manifests a damped vibration due to couplings to the environment. The maximum fidelity is more than 0.9 around the first peak at $t = \pi/\sqrt{2}\Omega_1 \simeq 0.17$ μs as a longer pulse duration yields more loss. When a nuclear spin in the second shell is to be polarized, the maximum fidelity is about 0.85, less than that for the nuclear spin in the first shell as the Rabi frequency is smaller due to a weaker hyperfine interaction. If we choose a nuclear spin even farther apart from the NV center, e.g., $A_\parallel = -7.5$ MHz, the maximum fidelity observably declines to 0.79. Because Rabi frequencies are limited by the large-detuning condition, the descending of maximum fidelity along with reducing of hyperfine interaction results from the increasing pulse duration. When the pure-dephasing rate κ is reduced from 1 to 1/5.8 MHz, e.g., Fig. 4(a) vs Fig. 4(b), an anomalous phenomenon occurs: the maximum fidelity achieved for the nuclear spin in the second shell is a little bit larger than that for the nuclear spin in the first shell. That is because the transverse hyperfine interaction provides an additional pathway for the intermediate state $|-,\uparrow\rangle$ to the nuclear-spin-polarized state $|0,\downarrow\rangle$. If the noise strength is further suppressed to $\kappa = 1/58$ MHz, e.g., Fig. 4(c), the first peak for a nuclear spin with $A_\parallel = -7.5$ MHz rises although more time is required for the evolution.

In the above investigations, we assume two-photon resonance to utilize the dark state to improve the transfer fidelity. In order to verify the constructive effect of dark state on the transfer, we plot the fidelity vs different two-photon detunings Δ in Fig. 5. As expected, the fidelity decreases along with the increase of Δ, as a larger Δ implies more component of $|E_1\rangle$ in the lossy intermediate state. In Fig. 5, the dependence of fidelity on the one-photon detuning δ is also explored. Similarly, the fidelity reduces monotonically as δ increases. In addition to the respective dynamical phases $\pm\Omega t$, which can be canceled by setting $\Omega t = \pi$, δt characterizes the synchronism of the two bright states with respect to the dark state. Because, in both cases, the maximum fidelity is achieved at the vanishing detuning, $\Delta = \delta = 0$ has been suggested for the optimal state transfer.

Generally speaking, in a practical experiment, there would be a small fluctuation in pulse amplitude. This imperfection leads to additional noise and obstacles for the implementation of quantum information processing, which can be overcome by dynamical decoupling with concatenated continuous driving and phase modulation [51,52]. Hereafter, by numerical

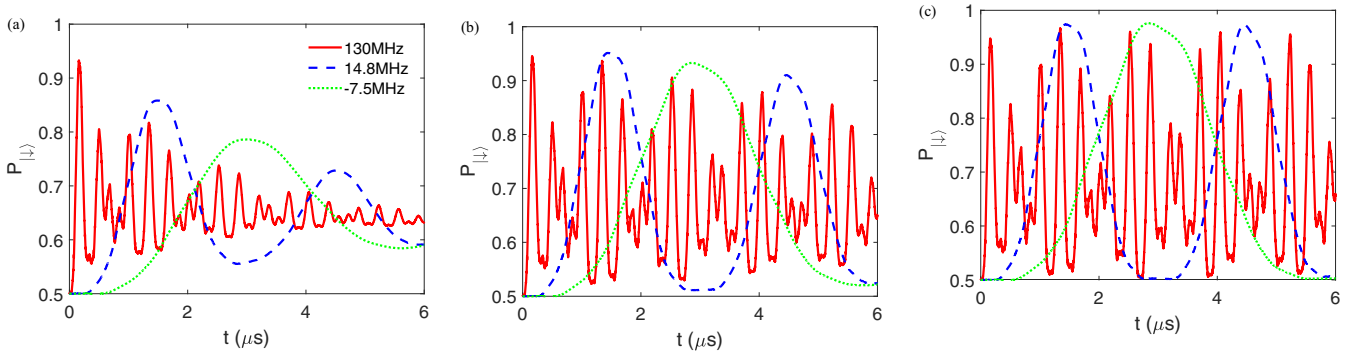

FIG. 4. The fidelity of nuclear spin in $|\downarrow\rangle$ vs $A_\parallel = A_\perp$ for different noise strength: (a) $\kappa = 1$ MHz, (b) $\kappa = 1/5.8$ MHz, and (c) $\kappa = 1/58$ MHz [50]. The solid red line is $A_\parallel = 130$ MHz [49], the dashed blue line is $A_\parallel = 14.8$ MHz [49], and the dotted green line is $A_\parallel = -7.5$ MHz [49].

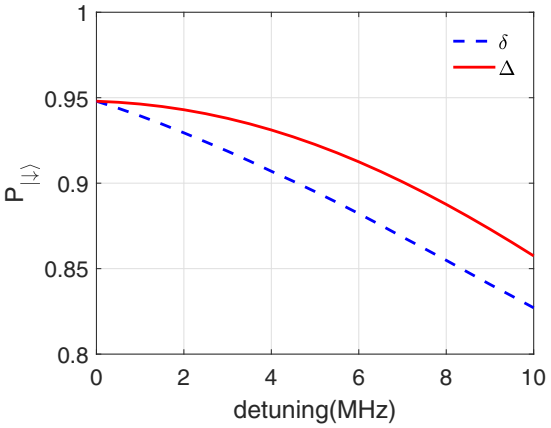

FIG. 5. The transfer fidelity $P_{|\downarrow\rangle}$ vs the one-photon (two-photon) detuning δ (Δ) for the first-shell ^{13}C. The dependence on Δ is shown by the red curve with $\delta = 0$. The dependence on δ is shown by the dashed blue curve with $\Delta = 0$. Other parameters are the same as in Fig. 2.

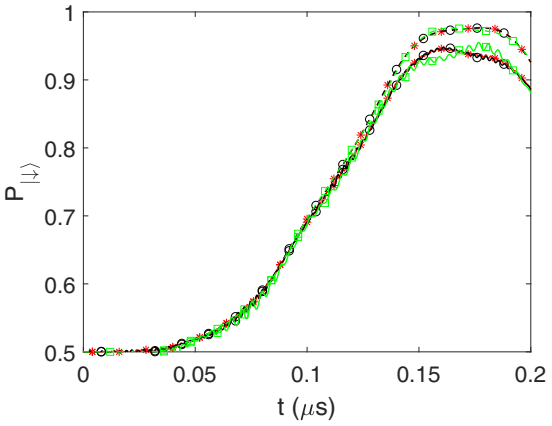

FIG. 7. The influence of magnetic field strength on the transfer fidelity for the first-shell ^{13}C: Red curves with stars for $B = 0$ G, black curves with circles for $B = 200$ G, and green curves with squares for $B = 1500$ G. The fidelity dynamics with (without) transverse hyperfine interaction is shown by the lower solid (upper dashed) curves. Other parameters are the same as in Fig. 2.

simulations, we demonstrate that our scheme is robust against the small fluctuation in the pulse amplitude. As shown in Fig. 6, the population dynamics with and without 1% amplitude fluctuation are compared. Since two species of curves almost coincide with each other, the maximum fidelity is hardly changed by the imperfect pulse. However, as the fluctuation increases, the noise in the pulse amplitude will inevitably reduce the fidelity, which is not shown here. In that case, the schemes proposed in Refs. [51,52] might play a role against the fluctuation in the pulse amplitude.

IV. DISCUSSION AND SUMMARY

The initialization of the nuclear spin is critical to the subsequent quantum information storage and processing. Facilitated by the strong hyperfine interaction with the electron spin, the nuclear spin in the vicinity of an NV center can be polarized by the swapping of the electron-spin polarization. And the swapping process is intrinsically a quantum-state process via a lossy intermediate state. In this paper, we propose to polarize the ^{13}C nuclear spin coupled to the electron spin of an NV center through the dark state. Our simulation demonstrates that the nuclear-spin polarization can reach about 97% for the next-next-nearest-neighbor site in the presence of small noises. In the following, we discuss the feasibility in the experiment and advantages of this proposal.

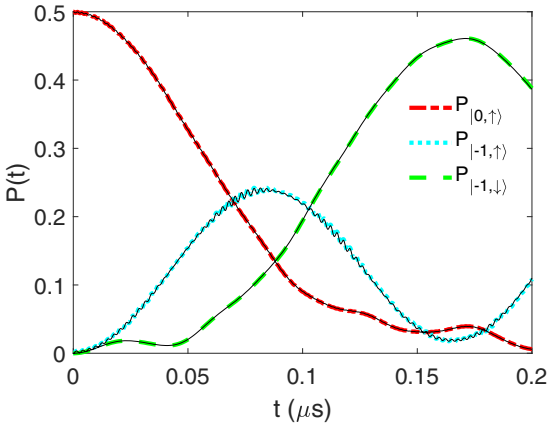

FIG. 6. The effect of pulse amplitude fluctuation on the population dynamics for the first-shell ^{13}C: dash-dotted red curve for $|0,\uparrow\rangle$, dotted blue curve for $|-,\uparrow\rangle$, and dashed green curve for $|-,\downarrow\rangle$. The population dynamics without 1% amplitude fluctuation is shown by the solid curves. Other parameters are the same as in Fig. 2.

In theory, in the case of stronger Rabi frequencies Ω_1 and Ω_2, it takes a shorter time t for the nuclear spin to reach the maximum polarization. In our scheme, the magnitudes of Ω_1 and Ω_2 are limited by the selective-excitation condition. The driving frequency ω_A is set to be in close resonance with the transition $|0,\uparrow\rangle \rightleftharpoons |-,\uparrow\rangle$, i.e., $\Omega_1 \gtrsim \delta$. On the other hand, the level spacing between $|0,\downarrow\rangle$ and $|-,\downarrow\rangle$ is $D - \gamma_e B_z + A_\parallel/2$. To selectively address the transition between $|0,\uparrow\rangle$ and $|-,\uparrow\rangle$, the Rabi frequency Ω_1 must satisfy the large-detuning condition, i.e., $\Omega_1 \ll \delta + A_\parallel$. In the same way, we can deduce that $\delta - \Delta \lesssim \Omega_2 \ll A_\parallel + \delta - \Delta - 2\gamma_c B_z$. To be specific, because the hyperfine interaction between the electronic spin and the ^{13}C nuclear spin in the first shell $A_\parallel$ is 130 MHz, the Rabi frequencies can be no more than 13 MHz. Furthermore, in order to validate the secular approximation, the magnetic field strength and the hyperfine interaction should fulfill the requirement $|D - \gamma_e B_z + \gamma_c B_z - \frac{1}{2}A_\parallel| \gg A_\perp/\sqrt{2}$. In other words, $B_z \leqslant 673$ G or $B_z \geqslant 1330$ G for the case with a ^{13}C nuclear spin in the first shell. In Fig. 7, the dynamics of fidelity is plotted vs different B. In order to verify the secular approximation, the dynamics with and without the transverse hyperfine interaction are compared. Although in all cases the curves without $A_\perp$ are slightly higher than those with $A_\perp$, the maximum fidelities are generally larger than 0.92. Therefore, our scheme is valid for a broad range of magnetic field, in contrast to the schemes based on the ground (excited) state level anticrossing, which are sensitive to both the magnitude and inclination of the magnetic field.

Compared with Refs. [27,34], our scheme does not require a specific magnetic field to result in a level anticrossing in the

ground or excited states. Besides, our proposal is not sensitive to the inclination of applied magnetic field. In Refs. [26,31], the initialization of nuclear spin with fidelity 85% is realized by mapping the electronic spin polarization into the nuclear spin state with a weak hyperfine interaction after ten repetitions. However, our proposal can reach about 97% in a weaker hyperfine interaction with one cycle which is much higher than theirs. In other words, to achieve the same effect, the repetitions of our proposal could be much fewer than ten cycles. And, it is more convenient than the single-shot readout approach in Refs. [28,29]. Furthermore, the effect of pure dephasing in our method can be further suppressed to reach an optimal result by the dynamical decoupling techniques [53–56].

ACKNOWLEDGMENTS

We thank Y. D. Wang and H. Dong for stimulating discussions. F.-G.D. was supported by the National Natural Science Foundation of China under Grant No. 11474026 and the Fundamental Research Funds for the Central Universities under Grant No. 2015KJJCA01. M.Z. was supported by the National Natural Science Foundation of China under Grant No. 11475021. J.-M.C. is supported by the National Natural Science Foundation of China (Grant No. 11574103), and the National Young 1000 Talents Plan. Q.A. was supported by the National Natural Science Foundation of China under Grant No. 11505007, and the Open Research Fund Program of the State Key Laboratory of Low-Dimensional Quantum Physics, Tsinghua University Grant No. KF201502.

Y.-Y.W., J.Q., and Y.-Q.C. contributed equally to this work.

APPENDIX: QUANTUM DYNAMICS AND DARK STATE

In the basis of $\{|0,\uparrow\rangle,|-,\uparrow\rangle,|-,\downarrow\rangle\}$, the Hamiltonian is written in the matrix form as

$$H=\begin{pmatrix}0 & \Omega_1 & 0\\ \Omega_1 & \omega_1 & \Omega_2\\ 0 & \Omega_2 & \omega_2\end{pmatrix}, \tag{A1}$$

where

$$\omega_1=\delta-i\kappa/2, \tag{A2}$$

$$\omega_2=\Delta-i\kappa/2. \tag{A3}$$

We consider the time evolution of an initial state $|\psi(0)\rangle=|0,\uparrow\rangle$. At any time, the state reads

$$|\psi(t)\rangle=u(t)|0,\uparrow\rangle+v(t)|-,\uparrow\rangle+w(t)|-,\downarrow\rangle. \tag{A4}$$

According to the Schrödinger equation, we obtain a set of differential equations for the probability amplitudes as

$$i\dot{u}(t)=\Omega_1 v(t), \tag{A5a}$$

$$i\dot{v}(t)=\Omega_1 u(t)+\omega_1 v(t)+\Omega_2 w(t), \tag{A5b}$$

$$i\dot{w}(t)=\Omega_2 v(t)+\omega_2 w(t), \tag{A5c}$$

with the initial condition $u(0)=1$, $v(0)=w(0)=0$. By Laplace transformation, $\tilde{\alpha}(p)=\int_0^\infty \alpha(t)e^{-pt}dt$ $(\alpha=u,v,w)$, we obtain

$$i[p\tilde{u}(p)-1]=\Omega_1\tilde{v}(p), \tag{A6a}$$

$$ip\tilde{v}(p)=\Omega_1\tilde{u}(p)+\omega_1\tilde{v}(p)+\Omega_2\tilde{w}(p), \tag{A6b}$$

$$ip\tilde{w}(p)=\Omega_2\tilde{v}(p)+\omega_2\tilde{w}(p), \tag{A6c}$$

or equivalently in the matrix form

$$\begin{bmatrix}-ip & \Omega_1 & 0\\ \Omega_1 & \omega_1-ip & \Omega_2\\ 0 & \Omega_2 & \omega_2-ip\end{bmatrix}\begin{bmatrix}\tilde{u}(p)\\ \tilde{v}(p)\\ \tilde{w}(p)\end{bmatrix}=\begin{bmatrix}-i\\ 0\\ 0\end{bmatrix}. \tag{A7}$$

We define

$$\det D\equiv\begin{vmatrix}-ip & \Omega_1 & 0\\ \Omega_1 & \omega_1-ip & \Omega_2\\ 0 & \Omega_2 & \omega_2-ip\end{vmatrix}$$

$$=(x_1-ip)(x_2-ip)(x_3-ip), \tag{A8a}$$

$$\det D_1\equiv\begin{vmatrix}-i & \Omega_1 & 0\\ 0 & \omega_1-ip & \Omega_2\\ 0 & \Omega_2 & \omega_2-ip\end{vmatrix}$$

$$=-i(\omega_1-ip)(\omega_2-ip)-(-i)\Omega_2^2, \tag{A8b}$$

$$\det D_2\equiv\begin{vmatrix}-ip & -i & 0\\ \Omega_1 & 0 & \Omega_2\\ 0 & 0 & \omega_2-ip\end{vmatrix}=i\Omega_1(\omega_2-ip), \tag{A8c}$$

$$\det D_3\equiv\begin{vmatrix}-ip & \Omega_1 & -i\\ \Omega_1 & \omega_1-ip & 0\\ 0 & \Omega_2 & 0\end{vmatrix}=-i\Omega_1\Omega_2, \tag{A8d}$$

where x_j's are the eigenenergies of Hamiltonian (A1), which are determined later. And thus we have

$$\tilde{u}(p)=\frac{\det D_1}{\det D}=-i\frac{(\omega_1-ip)(\omega_2-ip)-\Omega_2^2}{(x_1-ip)(x_2-ip)(x_3-ip)}, \tag{A9a}$$

$$\tilde{v}(p)=\frac{\det D_2}{\det D}=-i\frac{\Omega_1(ip-\omega_2)}{(x_1-ip)(x_2-ip)(x_3-ip)}, \tag{A9b}$$

$$\tilde{w}(p)=\frac{\det D_3}{\det D}=-i\frac{\Omega_1\Omega_2}{(x_1-ip)(x_2-ip)(x_3-ip)}. \tag{A9c}$$

Furthermore, by inverse Laplace transformation, $\alpha(t)=(2\pi i)^{-1}\int_{\sigma+i\infty}^{\sigma+i\infty}\tilde{\alpha}(p)e^{pt}dp$ $(\alpha=u,v,w)$, we obtain the probability amplitudes as

$$u(t)=\sum_{j=1}^{3}\frac{(x_j-\omega_1)(x_j-\omega_2)-\Omega_2^2}{\prod_{k\neq j}(x_j-x_k)}e^{-ix_jt}, \tag{A10a}$$

$$v(t)=\sum_{j=1}^{3}\frac{\Omega_1(x_j-\omega_2)}{\prod_{k\neq j}(x_j-x_k)}e^{-ix_jt}, \tag{A10b}$$

$$w(t)=\sum_{j=1}^{3}\frac{\Omega_1\Omega_2}{\prod_{k\neq j}(x_j-x_k)}e^{-ix_jt}. \tag{A10c}$$

According to the Schrödinger equation, the eigenenergies x_j's are the solutions to the following equation:

$$x[x^2 - (\omega_1 + \omega_2)x + \omega_1\omega_2 - \Omega^2] + \Omega_1^2\omega_2 = 0, \tag{A11}$$

where

$$\Omega^2 = \Omega_1^2 + \Omega_2^2. \tag{A12}$$

When ω_2 is small, assuming

$$x_j \simeq x_{0j} + A_j\omega_2, \tag{A13}$$

we can obtain the approximate solutions by the perturbation theory. The zero-order terms are determined by

$$x_{0j}\left[x_{0j}^2 - (\omega_1 + \omega_2)x_{0j} + \omega_1\omega_2 - \Omega^2\right] = 0, \tag{A14}$$

where

$$x_{01} = 0, \tag{A15a}$$
$$x_{02} = \omega_+, \tag{A15b}$$
$$x_{03} = \omega_-, \tag{A15c}$$
$$\omega_\pm = \tfrac{1}{2}[(\omega_1 + \omega_2) \pm \sqrt{(\omega_1 - \omega_2)^2 + 4\Omega^2}]. \tag{A15d}$$

Therefore, Eq. (A11) can be rewritten as

$$x(x - \omega_+)(x - \omega_-) + \Omega_1^2\omega_2 = 0. \tag{A16}$$

By inserting $x_1 = A_1\omega_2$ into Eq. (A16), to the zeroth order of ω_2, we obtain

$$A_1 = -\frac{\Omega_1^2}{\omega_+\omega_-} \simeq \frac{\Omega_1^2}{\Omega^2}. \tag{A17}$$

By inserting $x_2 = \omega_+ + A_2\omega_2$ into Eq. (A16), to the zeroth order of ω_2, we obtain

$$A_2 = -\frac{\Omega_1^2}{\omega_+(\omega_+ - \omega_-)} \simeq -\frac{\Omega_1^2}{2\Omega^2}. \tag{A18}$$

By inserting $x_3 = \omega_- + A_3\omega_2$ into Eq. (A16), to the zeroth order of ω_2, we obtain

$$A_3 = \frac{\Omega_1^2}{\omega_-(\omega_+ - \omega_-)} \simeq -\frac{\Omega_1^2}{2\Omega^2}. \tag{A19}$$

The eigenstates are

$$|E_i\rangle = \frac{1}{N_i}\Big\{\left[(x_i - \omega_1)(x_i - \omega_2) - \Omega_2^2\right]|0,\uparrow\rangle + \Omega_1(x_i - \omega_2)|-,\uparrow\rangle + \Omega_1\Omega_2|-,\downarrow\rangle\Big\}, \tag{A20}$$

where the normalization constants are given by

$$N_i^2 = \left|(x_i - \omega_1)(x_i - \omega_2) - \Omega_2^2\right|^2 + |\Omega_1(x_i - \omega_2)|^2 + |\Omega_1\Omega_2|^2. \tag{A21}$$

In the eigenbasis, the time evolution of the initial state $|\psi(0)\rangle = |0,\uparrow\rangle$ is

$$|\psi(t)\rangle = \sum_{j=1}^{3} \frac{N_j e^{-ix_j t}}{\prod_{k\neq j}(x_j - x_k)}|E_j\rangle. \tag{A22}$$

When $\omega_1,\omega_2 \ll \Omega_1,\Omega_2$, to the first order of ω_j's, we have

$$\begin{aligned}\omega_\pm &= \frac{1}{2}\left\{(\omega_1 + \omega_2) \pm \sqrt{4\Omega^2\left[1 + \frac{(\omega_1 - \omega_2)^2}{4\Omega^2}\right]}\right\} \\ &\simeq \frac{1}{2}\left\{(\omega_1 + \omega_2) \pm 2\Omega\left[1 + \frac{(\omega_1 - \omega_2)^2}{4\Omega^2}\right]\right\} \\ &\simeq \frac{1}{2}[(\omega_1 + \omega_2) \pm 2\Omega].\end{aligned} \tag{A23}$$

The eigenenergies are approximated to the first order of ω_j's as

$$x_1 \simeq \frac{\Omega_1^2}{\frac{1}{4}[4\Omega^2 - (\omega_1 + \omega_2)^2]}\omega_2 \simeq \frac{\Omega_1^2}{\Omega^2}\omega_2, \tag{A24a}$$

$$\begin{aligned}x_2 &\simeq \frac{1}{2}[(\omega_1 + \omega_2) + 2\Omega] - \frac{\Omega_1^2}{[(\omega_1 + \omega_2) + 2\Omega]\Omega}\omega_2 \\ &\simeq \Omega + \frac{1}{2}\left(\omega_1 + \frac{\Omega_2^2}{\Omega^2}\omega_2\right),\end{aligned} \tag{A24b}$$

$$\begin{aligned}x_3 &\simeq \frac{1}{2}[(\omega_1 + \omega_2) - 2\Omega] + \frac{\Omega_1^2}{[(\omega_1 + \omega_2) - 2\Omega]\Omega}\omega_2 \\ &\simeq -\Omega + \frac{1}{2}\left(\omega_1 + \frac{\Omega_2^2}{\Omega^2}\omega_2\right).\end{aligned} \tag{A24c}$$

Furthermore, the probability amplitudes can be obtained with the coefficients to the zeroth order of ω_j's and the phases to the first order of ω_j's as

$$\begin{aligned}u(t) &= \frac{(x_1 - \omega_1)(x_1 - \omega_2) - \Omega_2^2}{(x_1 - x_2)(x_1 - x_3)}e^{-ix_1 t} + \frac{(x_2 - \omega_1)(x_2 - \omega_2) - \Omega_2^2}{(x_2 - x_1)(x_2 - x_3)}e^{-ix_2 t} + \frac{(x_3 - \omega_1)(x_3 - \omega_2) - \Omega_2^2}{(x_3 - x_1)(x_3 - x_2)}e^{-ix_3 t} \\ &= \frac{(0 - \omega_1)(0 - \omega_2) - \Omega_2^2}{(0 - \omega_+)(0 - \omega_-)}e^{-i\frac{\Omega_1^2}{\Omega^2}\omega_2 t} + \frac{(\omega_+ - \omega_1)(\omega_+ - \omega_2) - \Omega_2^2}{(\omega_+ - 0)(\omega_+ - \omega_-)}e^{-i\left[\Omega + \frac{1}{2}\left(\omega_1 + \frac{\Omega_2^2}{\Omega^2}\omega_2\right)\right]t} \\ &\quad + \frac{(\omega_- - \omega_1)(\omega_- - \omega_2) - \Omega_2^2}{(\omega_- - 0)(\omega_- - \omega_+)}e^{-i\left[-\Omega + \frac{1}{2}\left(\omega_1 + \frac{\Omega_2^2}{\Omega^2}\omega_2\right)\right]t} \\ &= \frac{\Omega_2^2}{\Omega^2}e^{-i\frac{\Omega_1^2}{\Omega^2}\omega_2 t} + \frac{\Omega^2 - \Omega_2^2}{2\Omega^2}e^{-i\left[\Omega + \frac{1}{2}\left(\omega_1 + \frac{\Omega_2^2}{\Omega^2}\omega_2\right)\right]t} + \frac{\Omega^2 - \Omega_2^2}{2\Omega^2}e^{-i\left[-\Omega + \frac{1}{2}\left(\omega_1 + \frac{\Omega_2^2}{\Omega^2}\omega_2\right)\right]t} \\ &= \frac{\Omega_2^2}{\Omega^2}e^{-i\frac{\Omega_1^2}{\Omega^2}\omega_2 t} + \frac{\Omega_1^2}{\Omega^2}e^{-i\frac{1}{2}\left(\omega_1 + \frac{\Omega_2^2}{\Omega^2}\omega_2\right)t}\cos\Omega t,\end{aligned} \tag{A25}$$

$$
\begin{aligned}
v(t) &= \frac{\Omega_1(x_1-\omega_2)}{(x_1-x_2)(x_1-x_3)}e^{-ix_1t}+\frac{\Omega_1(x_2-\omega_2)}{(x_2-x_1)(x_2-x_3)}e^{-ix_2t}+\frac{\Omega_1(x_3-\omega_2)}{(x_3-x_1)(x_3-x_2)}e^{-ix_3t}\\
&= \frac{\Omega_1(0-\omega_2)}{(0-\Omega)(0+\Omega)}e^{-i\frac{\Omega_1^2}{\Omega^2}\omega_2t}+\frac{\Omega_1(\Omega-\omega_2)}{(\Omega-0)(\Omega+\Omega)}e^{-i\left[\Omega+\frac{1}{2}\left(\omega_1+\frac{\Omega_2^2}{\Omega^2}\omega_2\right)\right]t}+\frac{\Omega_1(-\Omega-\omega_2)}{(-\Omega-0)(-\Omega-\Omega)}e^{-i\left[-\Omega+\frac{1}{2}\left(\omega_1+\frac{\Omega_2^2}{\Omega^2}\omega_2\right)\right]t}\\
&= -i\frac{\Omega_1}{\Omega}e^{-i\frac{1}{2}\left(\omega_1+\frac{\Omega_2^2}{\Omega^2}\omega_2\right)t}\sin\Omega t, \qquad \text{(A26)}
\end{aligned}
$$

$$
\begin{aligned}
w(t) &\simeq \Omega_1\Omega_2\left\{\frac{e^{-i\frac{\Omega_1^2}{\Omega^2}\omega_2t}}{(0-\omega_+)(0-\omega_-)}+\frac{e^{-i\left[\Omega+\frac{1}{2}\left(\omega_1+\frac{\Omega_2^2}{\Omega^2}\omega_2\right)\right]t}}{(\omega_+-0)(\omega_+-\omega_-)}+\frac{e^{-i\left[-\Omega+\frac{1}{2}\left(\omega_1+\frac{\Omega_2^2}{\Omega^2}\omega_2\right)\right]t}}{(\omega_--0)(\omega_--\omega_+)}\right\}\\
&\simeq -\frac{\Omega_1\Omega_2}{\Omega^2}e^{-i\frac{\Omega_1^2}{\Omega^2}\omega_2t}+\frac{\Omega_1\Omega_2}{2\Omega^2}e^{-i\left[\Omega+\frac{1}{2}\left(\omega_1+\frac{\Omega_2^2}{\Omega^2}\omega_2\right)\right]t}+\frac{\Omega_1\Omega_2}{2\Omega^2}e^{-i\left[-\Omega+\frac{1}{2}\left(\omega_1+\frac{\Omega_2^2}{\Omega^2}\omega_2\right)\right]t}\\
&\simeq -\frac{\Omega_1\Omega_2}{\Omega^2}\left[e^{-i\frac{\Omega_1^2}{\Omega^2}\omega_2t}-e^{-i\frac{1}{2}\left(\omega_1+\frac{\Omega_2^2}{\Omega^2}\omega_2\right)t}\cos\Omega t\right]. \qquad \text{(A27)}
\end{aligned}
$$

When $\Omega t=\pi$,

$$
w(t)=-\frac{\Omega_1\Omega_2}{\Omega^2}\left[e^{-i\frac{\Omega_1^2}{\Omega^2}\frac{\pi}{\Omega}\omega_2}+e^{-i\frac{1}{2}\left(\omega_1+\frac{\Omega_2^2}{\Omega^2}\omega_2\right)\frac{\pi}{\Omega}}\right]=-\frac{\Omega_1\Omega_2}{\Omega^2}\left\{e^{-i\frac{\pi\Omega_1^2}{\Omega^3}(\Delta-i\frac{\kappa}{2})}+e^{-i\frac{1}{2}\left[\left(\delta+\frac{\Omega_2^2}{\Omega^2}\Delta\right)-i\left(1+\frac{\Omega_2^2}{\Omega^2}\right)\frac{\kappa}{2}\right]\frac{\pi}{\Omega}}\right\}. \qquad \text{(A28)}
$$

In order to obtain nearly complete polarization, the two following conditions should be fulfilled, i.e.,

$$
e^{-i\frac{\pi\Omega_1^2}{\Omega^3}\Delta}=e^{-i\frac{1}{2}\left(\delta+\frac{\Omega_2^2}{\Omega^2}\Delta\right)\frac{\pi}{\Omega}}, \qquad \text{(A29a)}
$$

$$
1\simeq e^{-\frac{\pi\Omega_1^2}{2\Omega^3}\kappa},e^{-\frac{\Omega^2+\Omega_2^2}{4\Omega^3}\pi\kappa}, \qquad \text{(A29b)}
$$

or equivalently

$$
\delta=\frac{2\Omega_1^2-\Omega_2^2}{\Omega^2}\Delta, \qquad \text{(A30a)}
$$

$$
\kappa\ll\frac{\Omega^3}{\pi\Omega_1^2},\frac{4\Omega^3}{\pi\left(\Omega^2+\Omega_2^2\right)}. \qquad \text{(A30b)}
$$

For $\Omega_1=\Omega_2$, we have

$$
\delta=\tfrac{1}{2}\Delta, \qquad \text{(A31a)}
$$

$$
\Omega\gg\tfrac{3}{8}\pi\kappa. \qquad \text{(A31b)}
$$

When the above condition is fulfilled, to the first order of κ, the polarization deviates from unity as

$$
\begin{aligned}
1-|\omega(t)|^2 &\simeq 1-\frac{\Omega_1^2\Omega_2^2}{\Omega^4}\left\{e^{-\frac{\pi\Omega_1^2}{\Omega^3}\kappa}+e^{-\left(1+\frac{\Omega_2^2}{\Omega^2}\right)\frac{\pi}{2\Omega}\kappa}+2\mathrm{Re}\left[e^{-i\frac{\pi\Omega_1^2}{\Omega^3}(\Delta-i\frac{\kappa}{2})}e^{i\frac{1}{2}\left[\left(\delta+\frac{\Omega_2^2}{\Omega^2}\Delta\right)+i\left(1+\frac{\Omega_2^2}{\Omega^2}\right)\frac{\kappa}{2}\right]\frac{\pi}{\Omega}}\right]\right\}\\
&= 1-\frac{\Omega_1^2\Omega_2^2}{\Omega^4}\left\{e^{-\frac{\pi\Omega_1^2}{\Omega^3}\kappa}+e^{-\left(1+\frac{\Omega_2^2}{\Omega^2}\right)\frac{\pi}{2\Omega}\kappa}+2\cos\left[-\frac{\pi\Omega_1^2}{\Omega^3}\Delta+\frac{1}{2}\left(\delta+\frac{\Omega_2^2}{\Omega^2}\Delta\right)\frac{\pi}{\Omega}\right]e^{-\frac{\pi\Omega_1^2}{2\Omega^3}\kappa}e^{-\frac{1}{4}\left(1+\frac{\Omega_2^2}{\Omega^2}\right)\frac{\pi}{\Omega}\kappa}\right\}\\
&\simeq 1-\frac{\Omega_1^2\Omega_2^2}{\Omega^4}\left\{1-\frac{\pi\Omega_1^2}{\Omega^3}\kappa+1-\left(1+\frac{\Omega_2^2}{\Omega^2}\right)\frac{\pi}{2\Omega}\kappa+2\left[1-\frac{\pi\Omega_1^2}{2\Omega^3}\kappa-\frac{1}{2}\left(1+\frac{\Omega_2^2}{\Omega^2}\right)\frac{\pi}{2\Omega}\kappa\right]\right\}\\
&= 1-\frac{\Omega_1^2\Omega_2^2}{\Omega^4}\left[4-2\frac{\pi\Omega_1^2}{\Omega^3}\kappa-2\left(1+\frac{\Omega_2^2}{\Omega^2}\right)\frac{\pi}{2\Omega}\kappa\right]=1-\left(1-\frac{\pi}{4\Omega}\kappa-\frac{3\pi}{8\Omega}\kappa\right)=\frac{5\pi}{8\Omega}\kappa. \qquad \text{(A32)}
\end{aligned}
$$

When both detunings vanish, i.e., $\Delta=\delta=0$, to the zeroth order of ω_j's, the eigenstates are

$$
|E_1\rangle\simeq\frac{1}{N_i}\left\{\left[(0-\omega_1)(0-\omega_2)-\Omega_2^2\right]|0,\uparrow\rangle+\Omega_1(0-\omega_2)|-,\uparrow\rangle+\Omega_1\Omega_2|-,\downarrow\rangle\right\}\simeq\frac{\Omega_2}{N_1}(-\Omega_2|0,\uparrow\rangle+\Omega_1|-,\downarrow\rangle), \qquad \text{(A33a)}
$$

$$
|E_2\rangle\simeq\frac{1}{N_2}\left\{\left[(\Omega-\omega_1)(\Omega-\omega_2)-\Omega_2^2\right]|0,\uparrow\rangle+\Omega_1(\Omega-\omega_2)|-,\uparrow\rangle+\Omega_1\Omega_2|-,\downarrow\rangle\right\}\simeq\frac{\Omega_1}{N_2}(\Omega_1|0,\uparrow\rangle+\Omega|-,\uparrow\rangle+\Omega_2|-,\downarrow\rangle), \qquad \text{(A33b)}
$$

$$|E_3\rangle \simeq \frac{1}{N_3}\{[(-\Omega-\omega_1)(-\Omega-\omega_2)-\Omega_2^2]|0,\uparrow\rangle+\Omega_1(-\Omega-\omega_2)|-,\uparrow\rangle+\Omega_1\Omega_2|-,\downarrow\rangle\}$$
$$\simeq \frac{\Omega_1}{N_3}(\Omega_1|0,\uparrow\rangle-\Omega|-,\uparrow\rangle+\Omega_2|-,\downarrow\rangle), \tag{A33c}$$

where the normalization constants are

$$N_1=\Omega_2\Omega, \tag{A34a}$$
$$N_2=N_3=\sqrt{2}\Omega_1\Omega. \tag{A34b}$$

Here $|E_1\rangle$ is the dark state because the probability in the lossy intermediate state $|-,\uparrow\rangle$ vanishes, while the other two are the bright states. The intermediate state $|-,\uparrow\rangle$ suffers from decoherence, and thus more probability in $|-,\uparrow\rangle$ results in less transfer fidelity. Because the probability amplitude of $|E_1\rangle$ in $|-,\uparrow\rangle$ is proportional to $x_1-\omega_2=\Omega_2^2(\Delta-i\kappa/2)/\Omega^2$ according to Eqs. (A3), (A20), and (A24a), the dark state does not exist unless the two-photon transition is resonant, i.e., $\Delta=0$. Notice that all expanding coefficients in the bright states are the same except there is a sign difference in the expanding coefficients of $|-,\uparrow\rangle$.

In the eigenbasis, the time evolution of the initial state $|\psi(0)\rangle=|0,\uparrow\rangle$ is

$$|\psi(t)\rangle=\frac{\Omega_2\Omega e^{-i\frac{\Omega_1^2}{\Omega^2}\omega_2 t}}{(0-\Omega)(0+\Omega)}|E_1\rangle+\frac{\sqrt{2}\Omega_1\Omega e^{-i\left[\Omega+\frac{1}{2}\left(\omega_1+\frac{\Omega_2^2}{\Omega^2}\omega_2\right)\right]t}}{(\Omega-0)(\Omega+\Omega)}|E_2\rangle+\frac{\sqrt{2}\Omega_1\Omega e^{-i\left[-\Omega+\frac{1}{2}\left(\omega_1+\frac{\Omega_2^2}{\Omega^2}\omega_2\right)\right]t}}{(-\Omega-0)(-\Omega-\Omega)}|E_3\rangle$$
$$=-\frac{\Omega_2 e^{-i\frac{\Omega_1^2}{\Omega^2}\omega_2 t}}{\Omega}|E_1\rangle+\frac{\sqrt{2}\Omega_1 e^{-i\frac{1}{2}\left(\omega_1+\frac{\Omega_2^2}{\Omega^2}\omega_2\right)t}}{2\Omega}(e^{-i\Omega t}|E_2\rangle+e^{i\Omega t}|E_3\rangle). \tag{A35}$$

Because there is a sign difference in the expanding coefficients of $|-,\uparrow\rangle$ in $|E_2\rangle$ and $|E_3\rangle$, the probability in $|-,\uparrow\rangle$ vanishes as long as $\Omega t=n\pi$ with n being an integer. To summarize, we utilize the dark state and quantum interference to achieve nearly complete polarization of the nuclear spin.

[1] V. V. Dobrovitski, G. D. Fuchs, A. L. Falk, C. Santori, and D. D. Awschalom, Quantum control over single spins in diamond, Annu. Rev. Condens. Matter Phys. **4**, 23 (2013).

[2] K. Nemoto, M. Trupke, S. J. Devitt, A. M. Stephens, B. Scharfenberger, K. Buczak, T. Nöbauer, M. S. Everitt, J. Schmiedmayer, and W. J. Munro, Photonic Architecture for Scalable Quantum Information Processing in Diamond, Phys. Rev. X **4**, 031022 (2014).

[3] M. A. Nielsen and I. L. Chuang, *Quantum Computation and Quantum Information* (Cambridge University Press, Cambridge, UK, 2000).

[4] G. D. Fuchs, V. V. Dobrovitski, D. M. Toyli, F. J. Heremans, and D. D. Awschalom, Gigahertz dynamics of a strongly driven single quantum spin, Science **326**, 1520 (2009).

[5] R. Hanson and D. D. Awschalom, Coherent manipulation of single spins in semiconductors, Nature (London) **453**, 1043 (2008).

[6] J.-M. Cai, A. Retzker, F. Jelezko, and M. B. Plenio, A large-scale quantum simulator on diamond surface at room temperature, Nat. Phys. **9**, 168 (2013).

[7] P. Andrich, C. F. de las Casas, X. Y. Liu, H. L. Bretscher, J. R. Berman, F. J. Heremans, P. F. Nealey, and D. D. Awschalom, Long-range spin wave mediated control of defect qubits in nanodiamonds, npj Quantum Inf. **3**, 28 (2017).

[8] H. Zhang, K. Arai, C. Belthangady, J. C. Jaskula, and R. L. Walsworth, Selective addressing of solid-state spins at the nanoscale via magnetic resonance frequency encoding, npj Quantum Inf. **3**, 31 (2017).

[9] M. W. Doherty, C. A. Meriles, A. Alkauskas, H. Fedder, M. J. Sellars, and N. B. Manson, Towards a Room-Temperature Spin Quantum Bus in Diamond via Electron Photoionization, Transport, and Capture, Phys. Rev. X **6**, 041035 (2016).

[10] P. E. Barclay, K.-M. C. Fu, C. Santori, A. Faraon, and R. G. Beausoleil, Hybrid Nanocavity Resonant Enhancement of Color Center Emission in Diamond, Phys. Rev. X **1**, 011007 (2011).

[11] D. M. Toyli, D. J. Christle, A. Alkauskas, B. B. Buckley, C. G. Van de Walle, and D. D. Awschalom, Measurement and Control of Single Nitrogen-Vacancy Center Spins above 600 K, Phys. Rev. X **2**, 031001 (2012).

[12] B. B. Buckley, G. D. Fuchs, L. C. Bassett, and D. D. Awschalom, Spin-light coherence for single-spin measurement and control in diamond, Science **330**, 1212 (2010).

[13] H. J. Mamin, M. Kim, M. H. Sherwood, C. T. Rettner, K. Ohno, D. D. Awschalom, and D. Rugar, Nanoscale nuclear magnetic resonance with a nitrogen-vacancy spin sensor, Science **339**, 557 (2013).

[14] J. F. Zhang, A. M. Souza, F. D. Brandao, and D. Suter, Protected Quantum Computing: Interleaving Gate Operations with Dynamical Decoupling Sequences, Phys. Rev. Lett. **112**, 050502 (2014).

[15] B. B. Zhou, A. Baksic, H. Ribeiro, C. G. Yale, F. J. Heremans, P. C. Jerger, A. Auer, G. Burkard, A. A. Clerk, and D. D. Awschalom, Accelerated quantum control using superadiabatic dynamics in a solid-state lambda system, Nat. Phys. **13**, 330 (2017).

[16] A. Baksic, H. Ribeiro, and A. A. Clerk, Speeding up Adiabatic Quantum State Transfer by Using Dressed States, Phys. Rev. Lett. **116**, 230503 (2016).

[17] J. F. Zhang, J. H. Shim, I. Niemeyer, T. Taniguchi, T. Teraji, H. Abe, S. Onoda, T. Yamamoto, T. Ohshima, J. Isoya, and D. Suter,

Experimental Implementation of Assisted Quantum Adiabatic Passage in a Single Spin, Phys. Rev. Lett. **110**, 240501 (2013).

[18] X.-K. Song, Q. Ai, J. Qiu, and F.-G. Deng, Physically feasible three-level transitionless quantum driving with multiple Schrödinger dynamics, Phys. Rev. A **93**, 052324 (2016).

[19] N. Zhao, J.-L. Hu, S.-W. Ho, J. T. K. Wan, and R. B. Liu, Atomic-scale magnetometry of distant nuclear spin clusters via nitrogen-vacancy spin in diamond, Nat. Nanotechnol. **6**, 242 (2011).

[20] T. van der Sar, Z. H. Wang, M. S. Blok, H. Bernien, T. H. Taminiau, D. M. Toyli, D. A. Lidar, D. D. Awschalom, R. Hanson, and V. V. Dobrovitski, Decoherence-protected quantum gates for a hybrid solid-state spin register, Nature (London) **484**, 82 (2012).

[21] H.-B. Liu, M. B. Plenio, and J.-M. Cai, Scheme for Detection of Single-Molecule Radical Pair Reaction Using Spin in Diamond, Phys. Rev. Lett. **118**, 200402 (2017).

[22] L. S. Li, H. H. Li, L. L. Zhou, Z. S. Yang, and Q. Ai, Measurement of weak static magnetic fields with nitrogen-vacancy color center, Acta Phys. Sin. **66**, 230601 (2017).

[23] N. Zhao, Z.-Y. Wang, and R.-B. Liu, Anomalous Decoherence Effect in a Quantum Bath, Phys. Rev. Lett. **106**, 217205 (2011).

[24] P. Huang, X. Kong, N. Zhao, F. Z. Shi, P. F. Wang, X. Rong, R.-B. Liu, and J. F. Du, Observation of an anomalous decoherence effect in a quantum bath at room temperature, Nat. Commun. **2**, 570 (2011).

[25] L. Childress, M. V. G. Dutt, J. M. Taylor, A. S. Zibrov, F. Jelezko, J. Wrachtrup, P. R. Hemmer, and M. D. Lukin, Coherent dynamics of coupled electron and nuclear spin qubits in diamond, Science **314**, 281 (2006).

[26] M. V. G. Dutt, L. Childress, L. Jiang, E. Togan, J. Maze, F. Jelezko, A. S. Zibrov, P. R. Hemmer, and M. D. Lukin, Quantum register based on individual electronic and nuclear spin qubits in diamond, Science **316**, 1312 (2007).

[27] V. Jacques, P. Neumann, J. Beck, M. Markham, D. Twitchen, J. Meijer, F. Kaiser, G. Balasubramanian, F. Jelezko, and J. Wrachtrup, Dynamic Polarization of Single Nuclear Spins by Optical Pumping of Nitrogen-Vacancy Color Centers in Diamond at Room Temperature, Phys. Rev. Lett. **102**, 057403 (2009).

[28] L. Jiang, J. S. Hodges, J. R. Maze, P. Maurer, J. M. Taylor, D. G. Cory, P. R. Hemmer, R. L. Walsworth, A. Yacoby, A. S. Zibrov, and M. D. Lukin, Repetitive readout of a single electronic spin via quantum logic with nuclear spin ancillae, Science **326**, 267 (2009).

[29] P. Neumann, J. Beck, M. Steiner, F. Rempp, H. Fedder, P. R. Hemmer, J. Wrachtrup, and F. Jelezko, Single-shot readout of a single nuclear spin, Science **329**, 542 (2010).

[30] P. C. Maurer, G. Kucsko, C. Latta, L. Jiang, N. Y. Yao, S. D. Bennett, F. Pastawski, D. Hunger, N. Chisholm, M. Markham, D. J. Twitchen, J. I. Cirac, and M. D. Lukin, Room-temperature quantum bit memory exceeding one second, Science **336**, 1283 (2012).

[31] J. H. Shim, I. Niemeyer, J. Zhang, and D. Suter, Room-temperature high-speed nuclear-spin quantum memory in diamond, Phys. Rev. A **87**, 012301 (2013).

[32] C. Zu, W.-B. Wang, L. He, W.-G. Zhang, C.-Y. Dai, F. Wang, and L.-M. Duan, Experimental realization of universal geometric quantum gates with solid-state spins, Nature (London) **514**, 72 (2014).

[33] J. F. Zhang and D. Suter, Experimental Protection of Two-Qubit Quantum Gates against Environmental Noise by Dynamical Decoupling, Phys. Rev. Lett. **115**, 110502 (2015).

[34] H.-J. Wang, C. S. Shin, C. E. Avalos, S. J. Seltzer, D. Budker, A. Pines, and V. S. Bajaj, Sensitive magnetic control of ensemble nuclear spin hyperpolarization in diamond, Nat. Commun. **4**, 1940 (2013).

[35] P. Neumann, N. Mizuochi, F. Rempp, P. Hemmer, H. Watanabe, S. Yamasaki, V. Jacques, T. Gaebel, F. Jelezko, and J. Wrachtrup, Multipartite entanglement among single spins in diamond, Science **320**, 1326 (2008).

[36] T. H. Taminiau, J. Cramer, T. van der Sar, V. V. Dobrovitski, and R. Hanson, Universal control and error correction in multi-qubit spin registers in diamond, Nat. Nanotechnol. **9**, 171 (2014).

[37] H. Dong, D. Z. Xu, J. F. Huang, and C. P. Sun, Coherent excitation transfer via the dark-state channel in a bionic system, Light: Sci. Appl. **1**, e2 (2012).

[38] Y. D. Wang and A. A. Clerk, Using Interference for High Fidelity Quantum State Transfer in Optomechanics, Phys. Rev. Lett. **108**, 153603 (2012).

[39] B. Khanaliloo, H. Jayakumar, A. C. Hryciw, D. P. Lake, H. Kaviani, and P. E. Barclay, Single-Crystal Diamond Nanobeam Waveguide Optomechanics, Phys. Rev. X **5**, 041051 (2015).

[40] D. A. Golter, T. Oo, M. Amezcua, I. Lekavicius, K. A. Stewart, and H. L. Wang, Coupling a Surface Acoustic Wave to an Electron Spin in Diamond via a Dark State, Phys. Rev. X **6**, 041060 (2016).

[41] A. Dréau, J.-R. Maze, M. Lesik, J.-F. Roch, and V. Jacques, High-resolution spectroscopy of single NV defects coupled with nearby ^{13}C nuclear spins in diamond, Phys. Rev. B **85**, 134107 (2012).

[42] D. Rugar, H. J. Mamin, M. H. Sherwood, M. Kim, C. T. Rettner, K. Ohno, and D. D. Awschalom, Proton magnetic resonance imaging using a nitrogen-vacancy spin sensor, Nat. Nanotechnol. **10**, 120 (2015).

[43] A. Dréau, P. Spinicelli, J. R. Maze, J.-F. Roch, and V. Jacques, Single-Shot Readout of Multiple Nuclear Spin Qubits in Diamond under Ambient Conditions, Phys. Rev. Lett. **110**, 060502 (2013).

[44] Q. Ai, Y. Li, H. Zheng, and C. P. Sun, Quantum anti-Zeno effect without rotating wave approximation, Phys. Rev. A **81**, 042116 (2010).

[45] J. R. Maze, P. L. Stanwix, J. S. Hodges, S. Hong, J. M. Taylor, P. Cappellaro, L. Jiang, M. V. Gurudev Dutt, E. Togan, A. S. Zibrov, A. Yacoby, R. L. Walsworth, and M. D. Lukin, Nanoscale magnetic sensing with an individual electronic spin in diamond, Nature (London) **455**, 644 (2008).

[46] A. Jarmola, V. M. Acosta, K. Jensen, S. Chemerisov, and D. Budker, Temperature- and Magnetic-Field-Dependent Longitudinal Spin Relaxation in Nitrogen-Vacancy Ensembles in Diamond, Phys. Rev. Lett. **108**, 197601 (2012).

[47] S. Takahashi, R. Hanson, J. van Tol, M. S. Sherwin, and D. D. Awschalom, Quenching Spin Decoherence in Diamond through Spin Bath Polarization, Phys. Rev. Lett. **101**, 047601 (2008).

[48] Q. Ai, Y.-J. Fan, B.-Y. Jin, and Y.-C. Cheng, An efficient quantum jump method for coherent energy transfer dynamics

in photosynthetic systems under the influence of laser fields, New J. Phys. **16**, 053033 (2014).

[49] B. Smeltzer, L. Childress, and A. Gali, ^{13}C hyperfine interactions in the nitrogen-vacancy centre in diamond, New J. Phys. **13**, 025021 (2011).

[50] T. A. Kennedy, J. S. Colton, J. E. Butler, R. C. Linares, and P. J. Doering, Long coherence times at 300 K for nitrogen-vacancy center spins in diamond grown by chemical vapor deposition, Appl. Phys. Lett. **83**, 4190 (2003).

[51] J.-M. Cai, B. Naydenov, R. Pfeiffer, L. P. McGuinness, K. D. Jahnke, F. Jelezko, M. B. Plenio, and A. Retzker, Robust dynamical decoupling with concatenated continuous driving, New J. Phys. **14**, 113023 (2012).

[52] D. Farfurnik, N. Aharon, I. Cohen, Y. Hovav, A. Retzker, and N. Bar-Gill, Experimental realization of time-dependent phase-modulated continuous dynamical decoupling, Phys. Rev. A **96**, 013850 (2017).

[53] G. de Lange, Z. H. Wang, D. Rist, V. V. Dobrovitski, and R. Hanson, Universal dynamical decoupling of a single solid-state spin from a spin bath, Science **330**, 60 (2010).

[54] B. Naydenov, F. Dolde, L. T. Hall, C. Shin, H. Fedder, L. C. L. Hollenberg, F. Jelezko, and J. Wrachtrup, Dynamical decoupling of a single-electron spin at room temperature, Phys. Rev. B **83**, 081201(R) (2011).

[55] C. A. Ryan, J. S. Hodges, and D. G. Cory, Robust Decoupling Techniques to Extend Quantum Coherence in Diamond, Phys. Rev. Lett. **105**, 200402 (2010).

[56] J. F. Du, X. Rong, N. Zhao, Y. Wang, J. H. Yang, and R. B. Liu, Preserving electron spin coherence in solids by optimal dynamical decoupling, Nature (London) **461**, 1265 (2009).